



Fibronectin–Integrin $\alpha 5$ Signaling in Vascular Complications of Type 1 Diabetes

Minghao Chen,^{1,2} Rui Hu,^{1,2,3} Cristina Cavinato,⁴ Zhenwu W. Zhuang,^{1,2} Jiasheng Zhang,^{1,2} Sanguk Yun,^{1,2} Pablo Fernandez Tussy,^{5,6} Abhishek Singh,^{5,6} Sae-Il Murtada,⁴ Keiichiro Tanaka,^{1,2} Min Liu,^{1,2,3} Carlos Fernández-Hernando,^{5,6} Jay D. Humphrey,^{4,5} and Martin A. Schwartz^{1,2,4,7}

Diabetes 2022;71:2020–2033 | <https://doi.org/10.2337/db21-0958>

Vascular complications are a major cause of illness and death in patients with type 1 diabetes (T1D). Diabetic vascular basement membranes are enriched in fibronectin (FN), an extracellular matrix protein that amplifies inflammatory signaling in endothelial cells through its main receptor, integrin $\alpha 5\beta 1$. Binding of the integrin $\alpha 5$ cytoplasmic domain to phosphodiesterase 4D5 (PDE4D5), which increases phosphodiesterase catalytic activity and inhibits antiinflammatory cAMP signaling, was found to mediate these effects. Here, we examined mice in which the integrin $\alpha 5$ cytoplasmic domain is replaced by that of $\alpha 2$ (integrin $\alpha 5/2$) or the integrin $\alpha 5$ binding site in PDE4D is mutated (PDE4D^{mut}). T1D was induced via injection of streptozotocin and hyperlipidemia induced via injection of PCSK9 virus and provision of a high-fat diet. We found that in T1D and hyperlipidemia, the integrin $\alpha 5/2$ mutation reduced atherosclerosis plaque size by ~50%, with reduced inflammatory cell invasion and metalloproteinase expression. Integrin $\alpha 5/2$ T1D mice also had improved blood-flow recovery from hindlimb ischemia and improved biomechanical properties of the carotid artery. By contrast, the PDE4D^{mut} had no beneficial effects in T1D. FN signaling through integrin $\alpha 5$ is thus a major contributor to diabetic vascular disease but not through its interaction with PDE4D.

Cardiovascular complications remain the major cause of morbidity and mortality in patients with type 1 diabetes

(T1D), with higher risks of atherosclerosis, peripheral arterial disease, hypertension, and vascular dysfunction (1,2). These conditions are often attributed to the adverse effects of hyperglycemia on the vascular system (3). Although connections between hyperglycemia and cardiovascular disease are well established, mechanisms are not well understood.

Changes in the extracellular matrix (ECM) have been implicated in the pathogenesis of several cardiovascular conditions (4). Fibronectin (FN) is deposited in the intima at atherosclerosis-prone sites prior to lesion formation, where it contributes to endothelial cell inflammation and atherosclerotic lesions (5,6). Previous studies showed that deleting plasma FN or cell-derived isoforms limit atherosclerosis in *Apoe*^{-/-} hyperlipidemic mice (7,8). However, deleting plasma FN also resulted in thinner fibrous caps and increased markers of plaque vulnerability, raising doubts about FN itself as a therapeutic target.

Our group previously showed that FN, through its main receptor integrin $\alpha 5\beta 1$, amplifies activation of NF- κ B and other inflammatory pathways in endothelial cell responses to disturbed flow, oxidized low-density lipoproteins, and IL-1 β , whereas the collagen/laminin receptor integrin $\alpha 2\beta 1$ inhibits inflammation (9,10). The FN–integrin $\alpha 5$ signaling axis is mediated at least in part by recruiting and activating phosphodiesterase 4D5 (PDE4D5; the major isoform in endothelial cells), which hydrolyzes

¹Yale Cardiovascular Research Center, Department of Internal Medicine, Yale School of Medicine, New Haven, CT

²Section of Cardiovascular Medicine, Yale School of Medicine, New Haven, CT

³Department of Cardiovascular Surgery, Renmin Hospital of Wuhan University, Wuhan, People's Republic of China

⁴Department of Biomedical Engineering, Yale University, New Haven, CT

⁵Vascular Biology and Therapeutics Program, Yale School of Medicine, New Haven, CT

⁶Departments of Comparative Medicine and Pathology, Yale Center for Molecular and Systems Metabolism, Yale School of Medicine, New Haven, CT

⁷Departments of Cell Biology and Biomedical Engineering, Yale University, New Haven, CT

Corresponding author: Martin A. Schwartz, martin.schwartz@yale.edu

Received 1 November 2021 and accepted 20 June 2022

This article contains supplementary material online at <https://doi.org/10.2337/figshare.20126132>.

M.C. and R.H. contributed equally to this work.

© 2022 by the American Diabetes Association. Readers may use this article as long as the work is properly cited, the use is educational and not for profit, and the work is not altered. More information is available at <https://www.diabetesjournals.org/journals/pages/license>.

the antiinflammatory mediator cAMP to facilitate inflammatory signaling (9). Replacing the integrin $\alpha 5$ intracellular domain with that of $\alpha 2$ (integrin $\alpha 5/2$) or mutating the integrin $\alpha 5$ -binding site of PDE4D (which affects all PDE4D isoforms and thus is termed PDE4D^{mut}) reduced inflammatory signaling in endothelial cells and, in hyperlipidemic mice, reduced atherosclerotic plaque size and increased markers of stability (11). Integrin $\alpha 5/2$ mice also showed improved recovery from hindlimb ischemia (HLI) after femoral artery ligation (11).

T1D is associated with dramatic thickening and stiffening of the endothelial basement membrane, with highly elevated FN content (4,12–15). Hyperglycemia stimulates FN gene expression both in vitro and in vivo (16–18). Reducing FN expression was reported to dampen basement membrane thickening and capillary loss in diabetic rats (19,20). However, whether proinflammatory signaling through the FN–integrin $\alpha 5$ –PDE4D5 axis contributes to artery disease in T1D is unknown.

We therefore examined the integrin $\alpha 5/2$ and PDE4D^{mut} mice in models of T1D atherosclerosis and peripheral arterial disease. Our results showed that the $\alpha 5/2$ mutation substantially ameliorated the vascular effects of T1D. FN signaling through integrin $\alpha 5\beta 1$ is thus a major driver of diabetic vascular complications. However, the PDE4D^{mut} mice had slightly worse outcomes, indicating that the beneficial effects are not mediated by PDE4D.

RESEARCH DESIGN AND METHODS

Animals

C57BL/6J mice were purchased from The Jackson Laboratory (stock no. 005680), and are herein referred to as wild-type (WT) mice. C57BL/6J integrin $\alpha 5/2$ chimera and PDE4D^{mut} mouse strains were constructed in our laboratory, as described (9,10). Mice were maintained in a light- and temperature-controlled environment with free access to food and water. All animal protocols were approved by the Yale University Institutional Animal Care and Use Committee.

Mouse T1D and Atherosclerosis Model

T1D in mice was induced by five consecutive intraperitoneal injections of streptozotocin (STZ; diluted in citrate buffer, pH 4.2–4.5, 50 mg/kg for male and 50 or 75 mg/kg for female mice; Sigma; S1030) at age 8 weeks. Control mice were injected with the same volume of citrate buffer. Mice with three consecutive blood glucose test results >300 mg/dL 2 weeks after the last STZ injection were considered to have T1D. At 4 weeks after the first STZ or buffer injection, murine PCSK9 adeno-associated virus (pAAV/D377Y-mPCSK9; 10^{11} copies) (21) produced by the Gene Therapy Program Vector Core at the University of Pennsylvania School of Medicine (Philadelphia, PA) was injected via tail vein. Mice were fed a high-fat diet (HFD; Clinton/Cybulsky high-fat rodent diet with regular

casein and 1.25% added cholesterol; Research Diet, D12108c) for the indicated times before sacrifice.

HLI Model, Laser Doppler, and Micro-Computed Tomography

Mice were anesthetized with a mixture of 1.5–2% isoflurane. The hair on the left thigh was removed with Nair lotion and the surgical area was disinfected. A 5 mm longitudinal incision was made in the left thigh. The distal femoral artery, proximal to the popliteal artery and saphenous artery, was ligated using 6–0 silk sutures (Syneture) before excision of the vessel between the distal end of the superficial epigastric artery and the trifurcation of the femoral artery into the descending genicular, popliteal, and saphenous branches. The venous structures and accompanying peripheral nerves were kept intact. The overlying skin was closed with 6–0 prolene sutures (Ethicon) and disinfected. At the end of the procedure, buprenorphine was administered subcutaneously at 0.05 mg/kg, once preemptively, then every 12 h for 72 h. The survival rate was 100%.

Laser Doppler imaging (model LDI2-IR modified for high resolution; Moor Instruments, Wilmington, DE) was used to assess hind-foot blood flow at 1 day before HLI surgery, at the time of surgery, and on days 0, 3, 7, and 14 post-HLI surgery. The mice were placed on top of a heating pad during scanning to minimize variation in body temperature. Perfusion of the hind foot was assessed within anatomically defined regions of interest. The degree of perfusion is displayed on a color scale, with dark blue indicating no perfusion and red indicating greatest perfusion. Doppler images were converted into histograms, the average blood flow in each histogram was calculated, and the blood-flow perfusion ratio was determined as the ratio of the HLI (left hindlimb) to non-HLI (right hindlimb) blood perfusion.

After mice were euthanized, the vasculature was flushed with 0.9% normal saline with papaverin 4 mg/L, adenosine 1 g/L for 3 min, followed by 2% paraformaldehyde for 5 min at 100 mmHg. Fresh home-made 20% bismuth nanoparticles mixed in 5% gelatin were used as a micro-computed tomography (micro-CT) contrast agent (~ 0.2 mL/10 g body weight), which was injected at 0.75 mL/min using an automatic injector (mechanical injector). The mice were then immediately chilled on ice for >30 min and immersion-fixed in 2% paraformaldehyde overnight. The peripheral vasculature in the ischemic hindlimb and the contralateral normal hindlimb was imaged with a high-resolution micro-CT imaging system (GE eXplore Locus SP), set to a 0.007-mm effective detector pixel size. Microview software (GE Healthcare) was used for initial reconstruction. An advanced workstation was used for three-dimensional reconstruction and segmentation of the whole hindlimb at the 21- μ m spatial resolution. Using the knee as the breakpoint, we divided the three-dimensional vasculature into 200 sections both in the thigh and in the calf regions. Quantification was performed with

National Institutes of Health ImageJ software. The data were expressed as vascular segment numbers, representing the total number of vessels, of specified diameter, counted in 200 z-sections for the thigh region and another 200 z-sections for the calf region.

Carotid Artery Mechanical Test

At 8 weeks after the first STZ or citric buffer injection, T1D, control, WT, and integrin α 5/2 male mice were euthanized by intraperitoneal injection of Beuthanasia-D (105 mg/kg). Carotid arteries were harvested, mounted on glass cannulas, and immersed in a temperature-controlled (37°C) oxygenated (95% O₂/5% CO₂) Krebs-Ringer bicarbonate-buffered solution containing 2.5 mmol/L CaCl₂. Samples were subjected to a biomechanical testing protocol using a custom, computer-controlled biaxial device (22). Carotid arteries were first preconditioned via two contractions at their in vivo axial length stimulated by 100 mmol/L KCl followed by a washout with the Krebs-Ringer solution. Next, we carried out a series of isobaric (luminal pressure, 90 mmHg) and axially isometric (measured sample-specific in vivo axial stretch) analyses. These consisted of the following: contraction with 100 mmol/L KCl, relaxation (KCl washed out); contraction with 1 μ mol/L nonselective α 1-adrenergic receptor agonist phenylephrine; endothelial cell (EC)-dependent relaxation with 10 μ mol/L followed by 100 μ mol/L acetylcholine (without washout); contraction with 1 mmol/L of the eNOS inhibitor N ω -nitro-L-arginine methyl ester (L-NAME; without washout); relaxed with two sequential concentrations (1 μ mol/L and 10 μ mol/L) of the endothelium-independent NO donor sodium nitroprusside. The diameter during the entire protocol was recorded and used for data analysis. At the end of the active mechanical protocols, the Ca²⁺-Krebs solution was replaced with a Ca²⁺-free Krebs solution to block all contractions while heating and oxygenation conditions were maintained. Biaxial biomechanical testing was then conducted to assess passive mechanical metrics, including stiffness and elastic energy storage, as described previously (23,24).

Blood Collection and Measurement

Blood samples were collected from atherosclerotic mice (including T1D-atherosclerosis and control-atherosclerosis mice), first via the facial vein on the same day as PCSK9 injection and again through the facial vein and heart punch at sacrifice. Consecutive blood samples were collected from the facial vein of the same mouse at the same time of day for five consecutive days. Blood samples were centrifuged at 18,400g at 4°C for 10 min, and then the supernatant serum was extracted carefully by pipet. Blood from the facial vein was immediately stored at -80°C for total serum cholesterol and triacylglycerides (TAGs) tests. Blood samples from the heart were stored at 4°C for <1 week before lipoprotein-fraction analysis. Total serum cholesterol was determined by cholesterol

oxidase/colorimetric assay (Abcam; 65390). Plasma TAG levels were measured with a commercially available kit (Wako Pure Chemicals). Distribution of TAGs in the plasma lipoprotein fractions was measured by fast protein liquid chromatography gel filtration with two Sepharose 6 HR 10/30 columns (Pharmacia Biotech), as described (25).

Mouse Tissue Staining, Histology, and Morphometric Analysis

Mice were euthanized with an overdose of isoflurane (Henry Schein) and perfused through the left ventricle with PBS and then 3.7% formaldehyde. The heart, whole aorta, calf and thigh muscles were carefully dissected and fixed in 3.7% formaldehyde overnight at 4°C, washed with PBS three times, dehydrated in 30% sucrose in PBS for 1 h, embedded in optimal cutting temperature (OCT) compound, and frozen on dry ice. Analysis of sections across atherosclerotic plaques was done according to American Heart Association guidelines as described by Daugherty et al. (26). Tissue blocks were cut into 8- μ m sections using a cryostat (Leica) and sections were stored at -20°C until use.

Hematoxylin and eosin (H&E), Oil Red O (ORO), and Picrosirius Red staining on OCT sections were done by Yale's Research Histology Laboratory using standard techniques (11) and images acquired using a Nikon 80i microscope.

For immunofluorescence, OCT sections were thawed, blocked with 5% goat serum/0.1% Triton X-100/PBS for 1 h at room temperature, and incubated with primary antibodies (anti-smooth muscle α -actin, 1:400, Sigma, C6198; anti-fibronectin, 1:200, Sigma, F3648; CD45, 1:100, BD Bioscience, 550539; CD68, 1:300, Abcam, ab955; MMP2, 1:200, Abcam, ab37150; MMP9, 1:200, Abcam, ab58803; CD31, 1:200, BD Bioscience, 553370; hypoxia-inducible factor 1 α [HIF1 α], 1:500, Novus Biologicals, NB100-479; phospho-VEGFR2, 1:500, Cell Signaling, 2478; phospho-eNOS, 1:500, BD Bioscience, 612392) in blocking buffer overnight at 4°C, washed three times with 0.1% Tween-20/PBS, and then incubated with secondary antibodies in blocking buffer at 1:200 dilution for 1 h at room temperature. Secondary antibodies (Invitrogen) were donkey anti-rabbit, -rat, or -mouse, labeled with Alexafluor 488, 568, or 647. Slides were washed three times and mounted in DAPI Fluoromount G (Southern Biotech; 0100-20). Images were acquired on a Nikon 80i microscope or a Leica SP8 confocal microscope with the Leica Application Suite software.

For whole aorta ORO staining, the formaldehyde-fixed whole aorta was opened longitudinally, pinned en face on a soft-bottomed dish, briefly rinsed with 78% methanol, incubated with ORO solution (0.2% ORO in 7:2 methanol:1 M NaOH), and then washed in 78% methanol three times. The whole aorta was photographed with a digital microscopic camera (Leica DFC295).

Quantification and Statistical Analysis

ImageJ software (version 1.51; National Institutes of Health, Bethesda, MD) was used for morphometric analysis. Relative lesion area and positive staining area were calculated. Graphs were created using GraphPad Prism 6.0 software, and statistical analysis was performed using Student *t* test, one-way ANOVA, or two-way ANOVA, as described in the figure legends. Data are presented as mean \pm SEM; $P < 0.05$ was considered statistically significant.

Data and Resource Availability

The data sets generated and/or analyzed during this study are available from the corresponding author upon reasonable request. No applicable resources were generated or analyzed during the current study.

RESULTS

General Characterization of Mice With T1D and Hyperlipidemia

A preliminary experiment revealed that female mice required a higher STZ dose to achieve T1D (Supplementary Fig. 1), which resulted in very high mortality (32 of 34 female mice died before the end of the experiment) (Supplementary Table 1). We therefore used male mice for subsequent analyses. The protocol for induction of T1D and hyperlipidemia in mice is summarized in Fig. 1A. WT, integrin $\alpha 5/2$, and PDE4D5^{mut} mice received injections of STZ or citrate buffer and PCSK9 as indicated, then were placed on a HFD. In Figs. 1–3, WT mice that received citrate buffer/PCSK9/HFD were WT controls; WT, integrin $\alpha 5/2$ and PDE4D5^{mut} mice that received STZ/PCSK9/HFD were T1D mice.

WT control mice gained weight over the 8 weeks of HFD, whereas T1D mice did not (Fig. 1B). Blood glucose levels were elevated after STZ injection, with no differences among the three strains (Fig. 1C). WT T1D and integrin $\alpha 5/2$ T1D mice died at similar rates over the 8 weeks after PCSK9 injection, with poorer survival of the PDE4D5^{mut} strain (Fig. 1D). Serum cholesterol levels after PCSK9 injection and HFD increased more in T1D mice than in control mice with no difference among the three strains (Fig. 1E). Among the mice on the STZ/PCSK9/HFD regimen, the integrin $\alpha 5/2$ group had significantly lower TAG levels compared with the WT and PDE4D5^{mut} groups (Fig. 1F).

To further define the lower TAG levels observed in integrin $\alpha 5/2$ T1D mice, we measured TAG levels in lipoprotein fractions (i.e., VLDL, LDL/IDL, and HDL) isolated by fast-protein liquid chromatography, which showed reduced circulating TAG levels in VLDL fractions in integrin $\alpha 5/2$ T1D mice compared with WT T1D mice (Fig. 1G). It is known that blood TAG levels in patients with T1D can show large fluctuations. We therefore made serial measurements of TAG levels in another set of hyperlipidemic T1D integrin $\alpha 5/2$ and WT mice after 4 weeks of the HFD, collecting blood samples at the same time every day

for 5 days. TAG levels in each mouse varied only modestly over time (Supplementary Fig. 2A).

T1D–Atherosclerosis Model

To evaluate atherosclerosis after 8 weeks of the HFD, we examined two well-characterized atherosclerosis-prone regions: the aortic root and brachiocephalic artery. Quantitative morphometry of both H&E and ORO staining showed that all three strains of T1D mice developed larger atherosclerotic lesions than did WT control mice at both regions (Fig. 2A–F). However, integrin $\alpha 5/2$ T1D mice showed markedly smaller lesions relative to WT and PDE4D5^{mut} T1D mice. Similar results were observed between WT and integrin $\alpha 5/2$ T1D groups when the whole aorta was assessed by en face ORO staining (Fig. 2G and H).

To address whether the lower TAG level in integrin $\alpha 5/2$ T1D mice accounted for the reduction of atherosclerosis plaque, we extracted a cohort of WT versus integrin $\alpha 5/2$ T1D mice ($n = 7$ WT and 7 $\alpha 5/2$ mice) with equivalent TAG levels (Supplementary Fig. 2B) and found that these integrin $\alpha 5/2$ T1D mice consistently showed significantly reduced plaque size at the aortic root than WT T1D mice (Supplementary Fig. 2C). These results argue that differences in TAG levels do not account for the differences in disease in WT versus integrin $\alpha 5/2$ mice, though circulating TAGs are likely to contribute.

Leukocyte recruitment and ECM degradation play critical roles in plaque vulnerability (27,28). We therefore stained sections of the aortic root for CD45 (a general marker for hematopoietic cells) and CD68 (a marker for macrophages). Plaques in the aortic roots of WT and PDE4D5^{mut} T1D mice had more CD45- and CD68-positive cells than did those of WT control mice, but this effect was nearly abolished in integrin $\alpha 5/2$ T1D mice (Fig. 3A–C). MMP9 and MMP2 ECM-degrading proteinases secreted by the inflammatory cells destabilize plaques (29). The MMP9-positive area was significantly increased in the aortic root of WT T1D mice compared with that of nondiabetic WT mice (Fig. 3D and E). This increase was essentially abolished in integrin $\alpha 5/2$ T1D mice, whereas PDE4D5^{mut} T1D mice showed no improvement. Results for MMP2 yielded a similar trend as for MMP9, though the difference did not reach statistical significance (Fig. 3F).

Vascular smooth muscle cells (SMCs) synthesize a large fraction of the collagen in the fibrous cap and promote plaque stability. We therefore stained aortic root sections for smooth muscle α actin (SMA). WT T1D mice had greater SMA staining in the plaque compared with WT control mice, perhaps in keeping with larger plaques (Fig. 3G and H). SMA staining was similar between integrin $\alpha 5/2$ T1D mice and WT T1D mice. However, SMA content in PDE4D5^{mut} T1D plaques was $\sim 50\%$ lower (Fig. 3H). Fibrous cap thickness, FN staining, and Picrosirius red staining (for collagen) were increased in the T1D mice

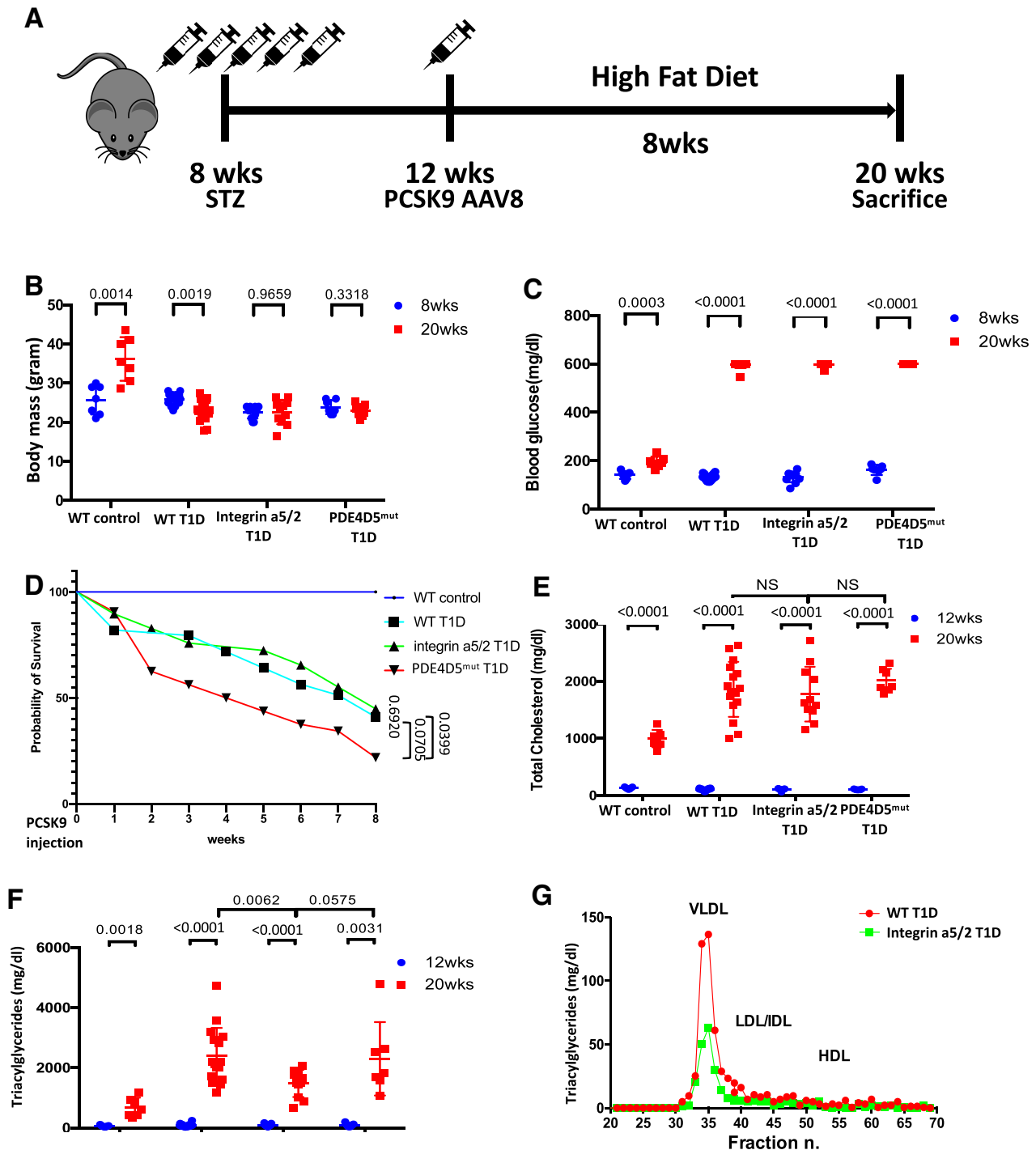


Figure 1—Experimental design and characterization of animals. (A) Schematic of T1D and hyperlipidemia mouse model design. (B) Body mass of animals at 8 and 20 weeks of age. (C) Blood glucose levels of animals at 8 and 20 weeks. (D) Survival curve for WT control, WT T1D, integrin $\alpha 5/2$ -T1D, and PDE4D^{mut} T1D mice. Analysis was by nonlinear regression. (E) Serum cholesterol concentration at 12 and 20 weeks. (F) Serum triglyceride (TAG) level at 12 and 20 weeks. (G) Lipoprotein profile of pooled plasma of WT and integrin $\alpha 5/2$ -T1D mice ($n = 5$ for each group). Student t test was used for analysis. (B–E and G) WT control, $n = 7$ mice; WT T1D, $n = 16$; integrin $\alpha 5/2$ T1D, $n = 11$; and PDE4D^{mut} T1D, $n = 7$. (B, C, E, and F) Student t test was used for comparing the same group before and after HFD. (E and F) One-way ANOVA was used for comparing different groups. Ctrl, control; DB, diabetic.

relative to nondiabetic mice, with no significant differences among the WT, integrin $\alpha 5/2$, and PDE4D^{mut} T1D groups (Fig. 3G and I and Supplementary Fig. 4A–D).

HLI and Blood Flow Recovery

Recovery from HLI after femoral artery ligation is commonly used to model peripheral arterial disease (30) and

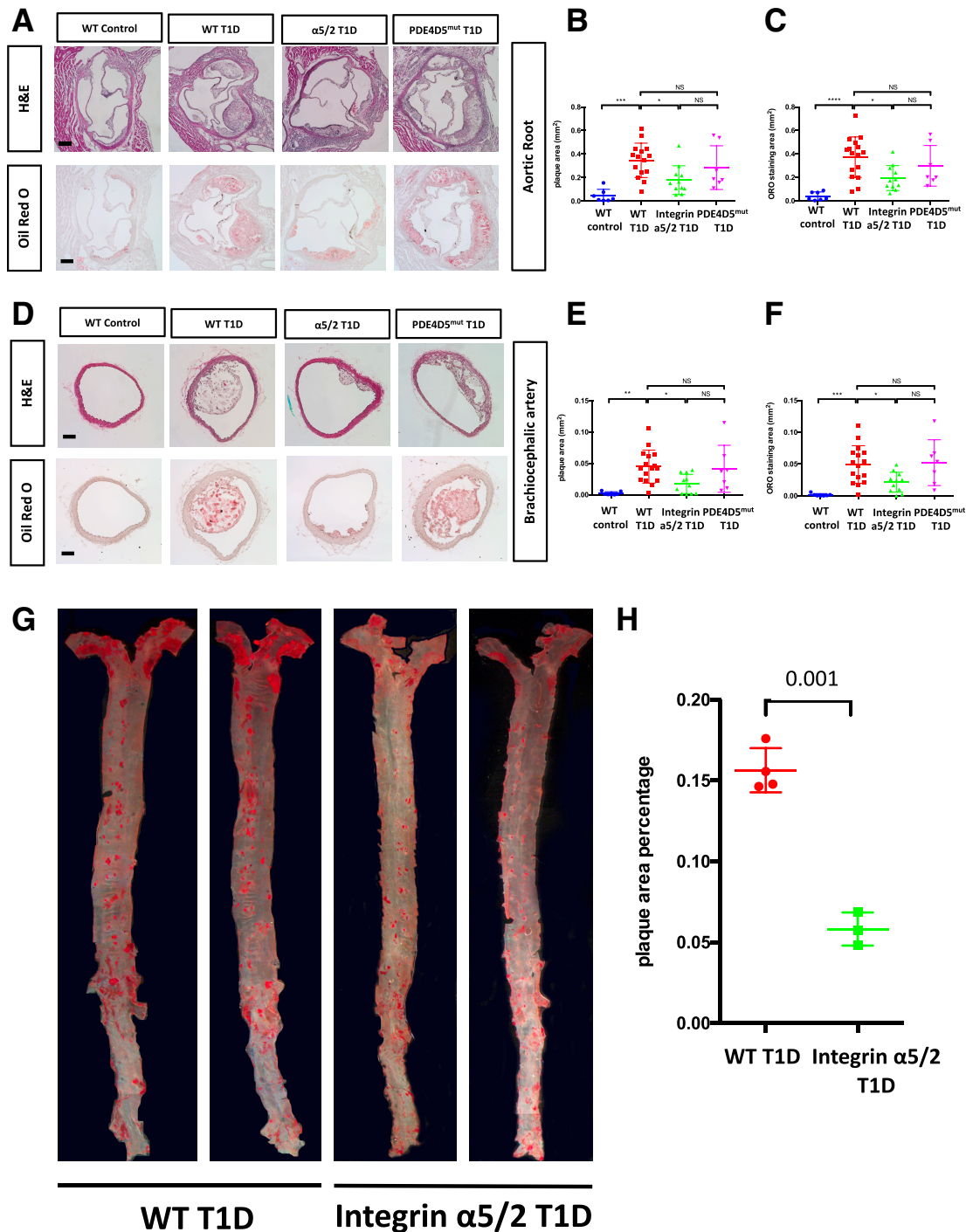


Figure 2—Atherosclerosis in arteries from mice injected with PCSK9 virus and placed on a HFD for 8 weeks. (A) Representative images of H&E and ORO staining of aortic root sections. (B) Quantification of plaque area of H&E staining in A. (C) Quantification of aortic root ORO staining area in A. (D) H&E and ORO staining of brachiocephalic artery (BCA) cross sections. (E) Quantification of BCA plaque area of H&E staining in D. (F) Quantification of BCA ORO-positive area in D. (G) Representative images of en face preparations of WT T1D and integrin α5/2 T1D aortas stained with ORO. (H) Quantification of ORO-positive area to whole area ratio in G. Analysis was by Student *t* test. (A–F) WT control, *n* = 7 mice. WT T1D, *n* = 16 mice; integrin α5/2 T1D, *n* = 11; and PDE4D^{mut} T1D, *n* = 7. (G and H) WT T1D, *n* = 4 mice; integrin α5/2 T1D, *n* = 3. (B, C, E, and F) One-way ANOVA was used. Ctrl, control.

is impaired in diabetic mice (31–34). Blood-flow recovery is primarily mediated by arteriogenesis in the thigh, induced by the increased shear stress in smaller arteries

parallel to the blockage, and also by angiogenesis in the calf, induced by angiogenic factors such as vascular endothelial growth factor (VEGF) secreted in response to hypoxia

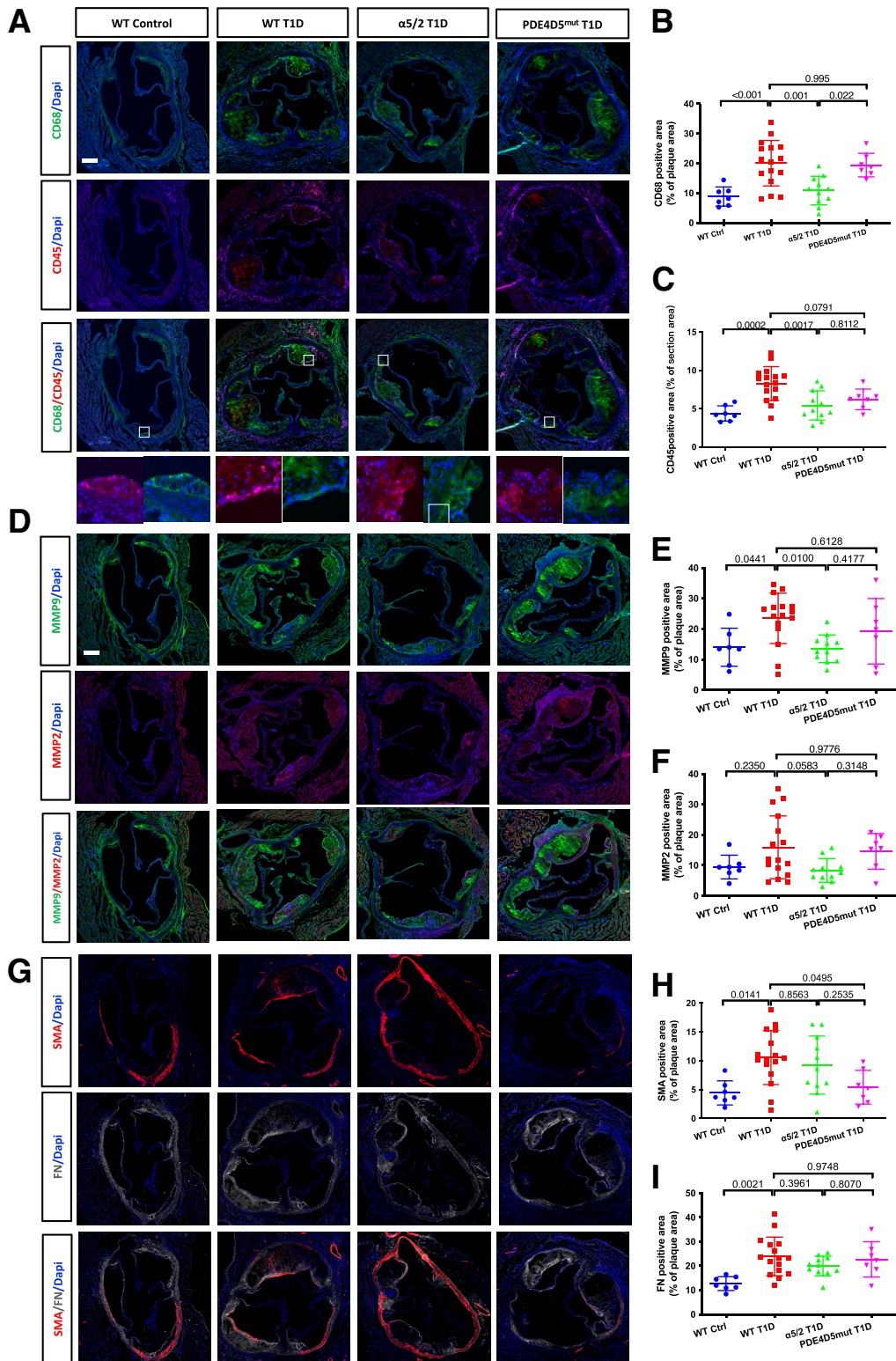


Figure 3—Plaque phenotype. (A) Representative images of CD68 and CD45 immunofluorescence (IF) staining of aortic root sections. (B) Quantification of CD68-positive area. (C) Quantification of CD45-positive area. (D) Representative images of MMP9 and MMP2 IF staining of aortic root sections. (E) Quantification of MMP9-positive area. (F) Quantification of MMP2-positive area. (G) Representative images of SMA and FN IF staining of aortic root sections. (H) Quantification of SMA-positive area. (I) Quantification of FN-positive area. WT control, $n = 7$ mice; WT T1D, $n = 16$; integrin $\alpha 5/2$ T1D, $n = 11$; and PDE4D^{mut} T1D, $n = 7$. (B, C, E, F, H, and I) One-way ANOVA was used. Ctrl, control.

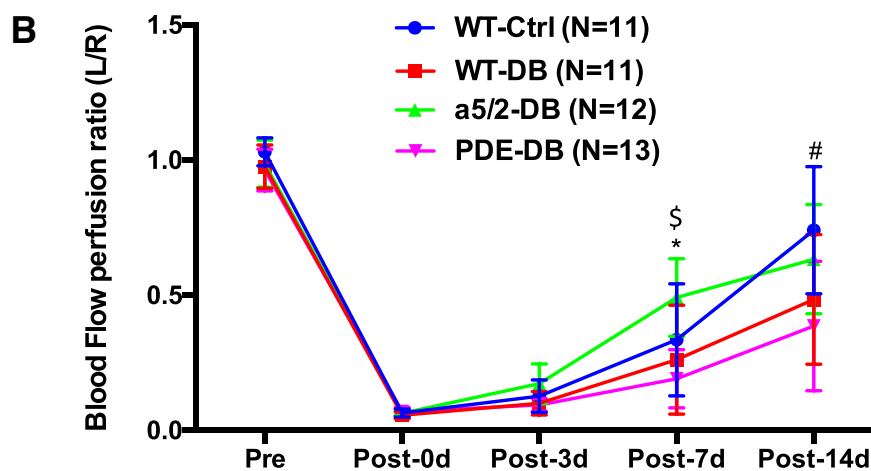
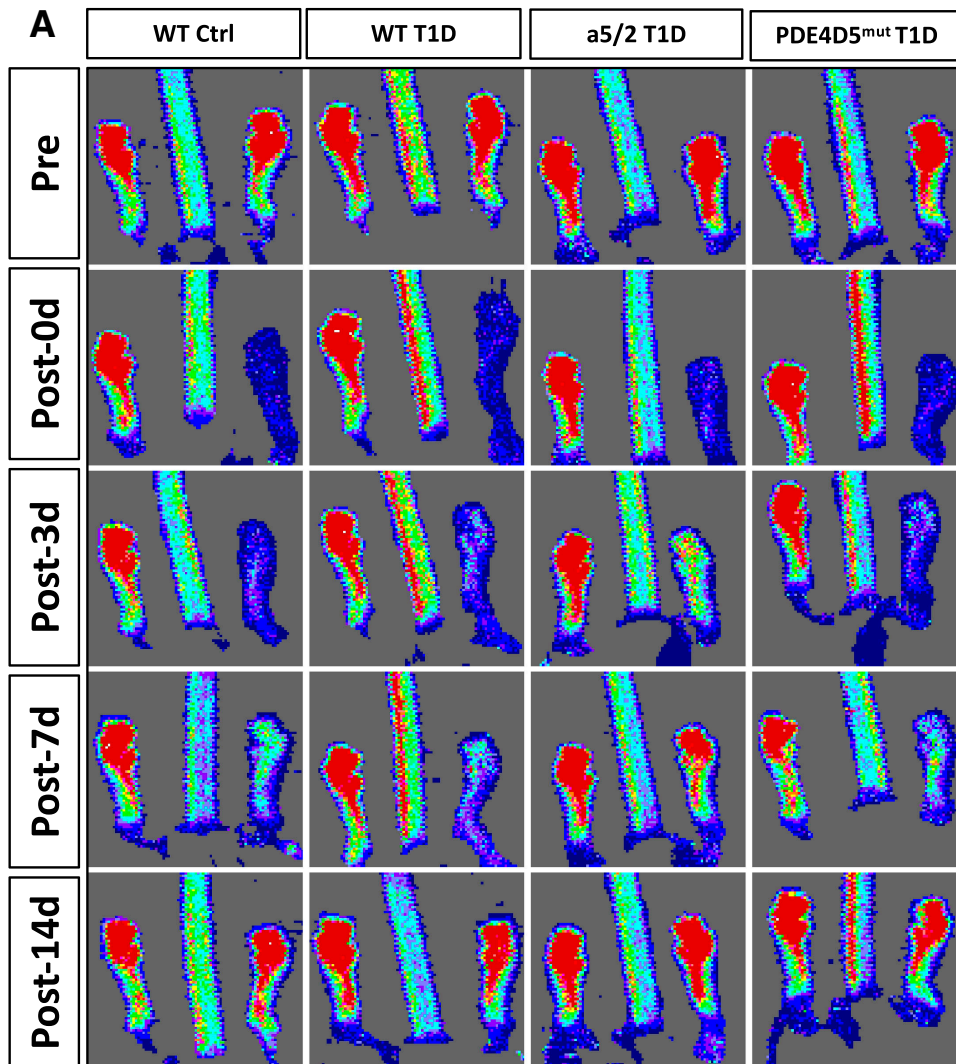


Figure 4—Blood-flow recovery after HLI surgery. (A) Representative laser Doppler image of blood flow before and after HLI. (B) Quantification of ratio of blood flow in the ischemic to the control foot measured by laser Doppler scan at indicated times. Analysis was by one-way ANOVA. WT control, $n = 11$ mice; WT T1D, $n = 11$; integrin $\alpha 5/2$ T1D, $n = 12$; and PDE4D^{mut} T1D, $n = 13$. *Between WT T1D and integrin $\alpha 5/2$ T1D, $P < 0.003$; §between integrin $\alpha 5/2$ T1D and PDE4D^{mut} T1D, $P < 0.0027$; #between integrin $\alpha 5/2$ T1D and PDE4D^{mut} T1D, $P < 0.0474$. Ctrl, control.

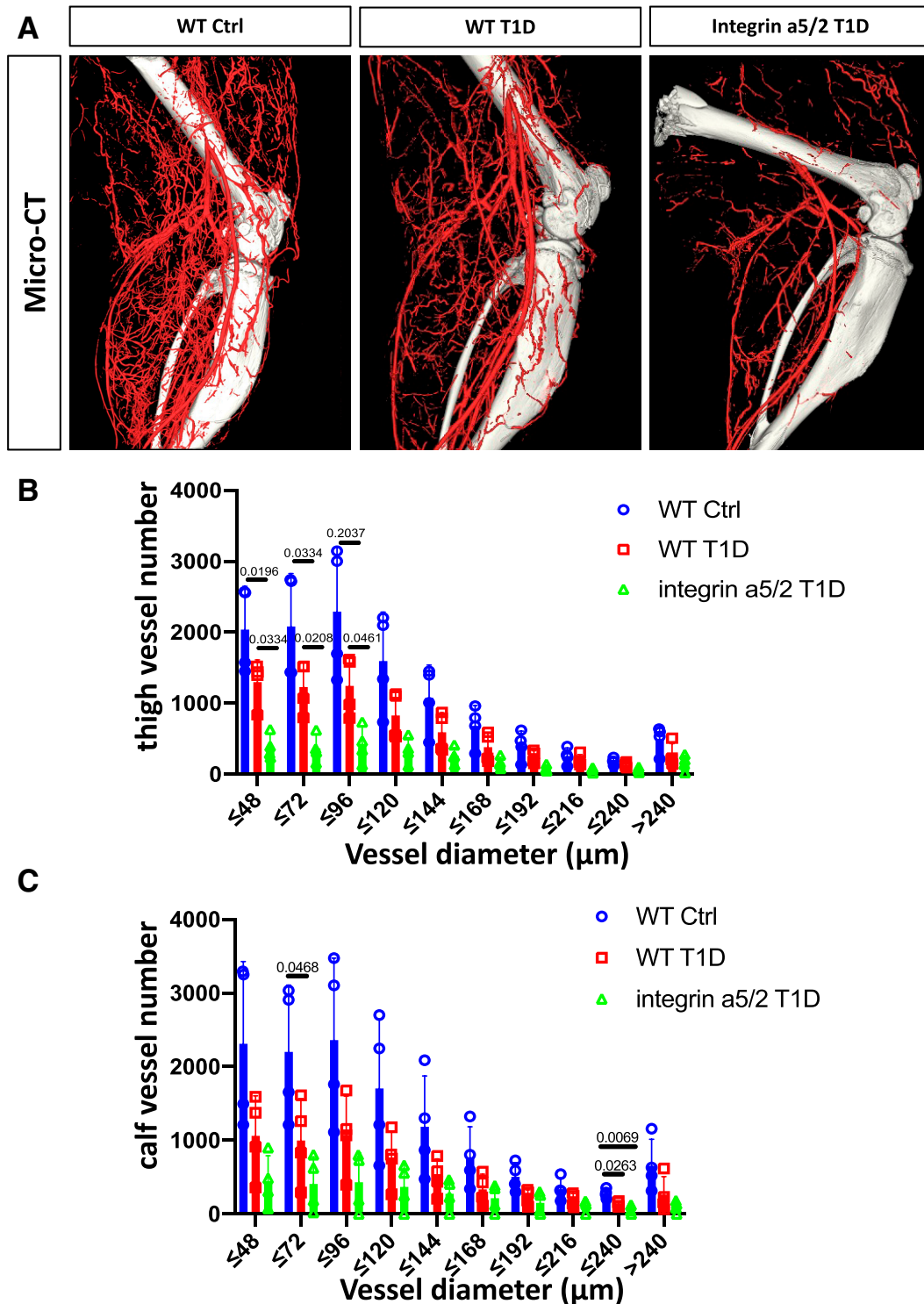


Figure 5—Micro-CT 14 days after HLI surgery. (A) Representative micro-CT images of artery casts at 14 days after HLI surgery. Quantification of blood vessels of diameters in the thigh (B) and the calf (C). (B and C) Data analysis was by one-way ANOVA. Ctrl, control.

(35). In Figs. 4–7, WT mice that received citrate buffer injections were WT controls; WT, integrin $\alpha 5/2$, and PDE4D5^{mut} mice that received consecutive STZ injections were T1D mice.

After ligation of the left femoral artery, we monitored blood flow in both hind feet by laser Doppler imaging,

using the unoperated right leg as a control. Immediately after surgery and 3 days after surgery, blood flow in the ligated leg was similar among the four groups. At 7 and 14 days after the surgery, blood-flow recovery was slower in WT T1D mice compared with WT control mice, as expected (Fig. 4A and B). However, integrin $\alpha 5/2$ T1D mice

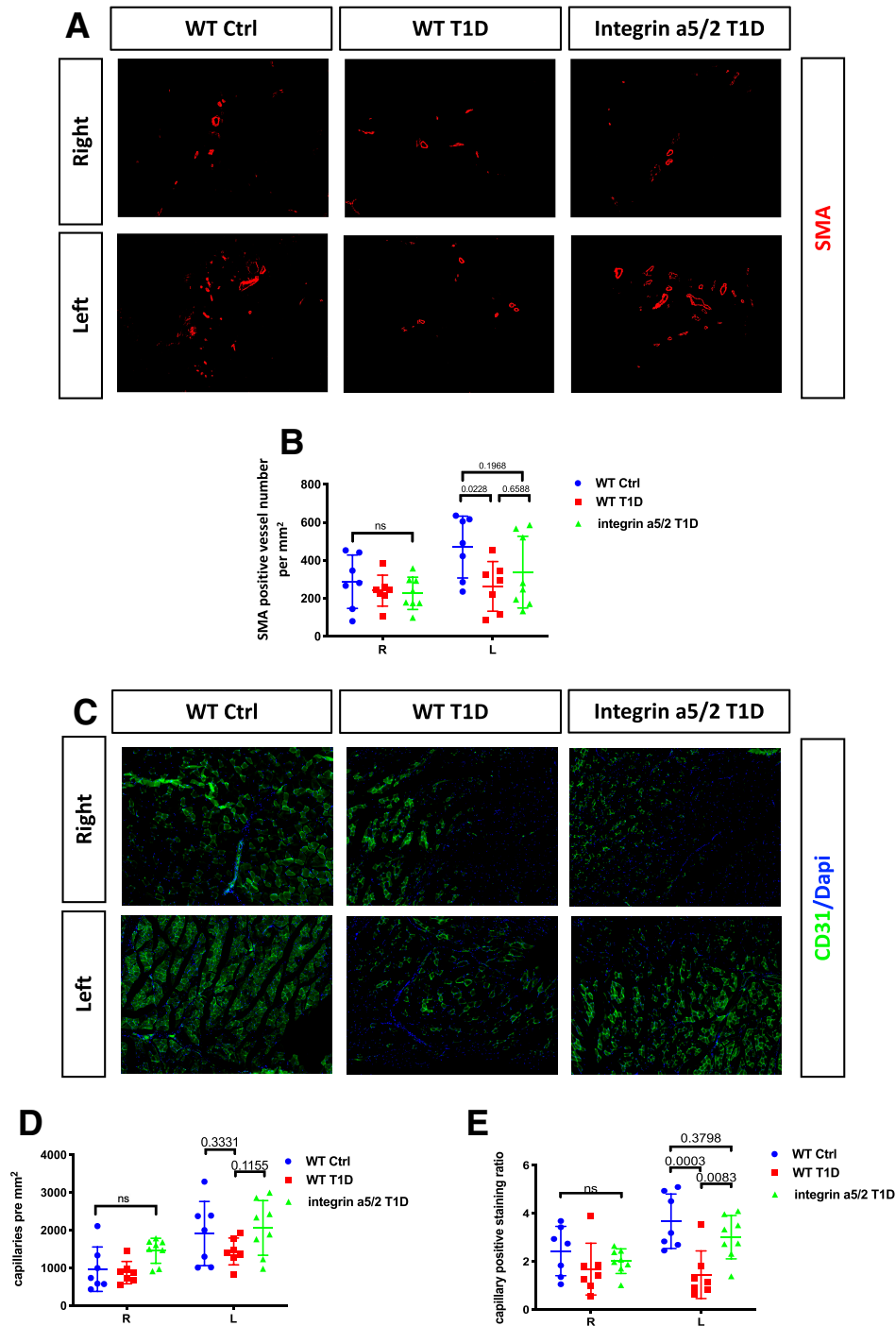


Figure 6—Arteriogenesis and angiogenesis 14 days after femoral artery ligation. (A) Representative images of SMA staining of sections from ligated and control thighs. (B) Quantification of SMA-positive vessel number per mm². (C) Representative images of CD31 staining of sections from

had significantly better flow recovery relative to WT T1D at 7 and 14 days. PDE4D5^{mut} T1D mice had the slowest blood-flow recovery over the entire time course.

The improved blood-flow recovery in integrin α5/2 T1D mice relative to WT T1D mice prompted us to address the mechanism. We therefore examined artery morphology of the ligated leg (i.e., the left side) at 14 days

postsurgery by micro-CT angiograms that label only the arterial network (diameter, 48–240 μm). In this procedure, arteries are maximally vasodilated prior to casting. As expected, WT T1D mice had fewer small arteries in the thigh compared with nondiabetic mice, consistent with poor arteriogenesis. To our surprise, integrin α5/2 T1D mice had even fewer arteries in this range compared with

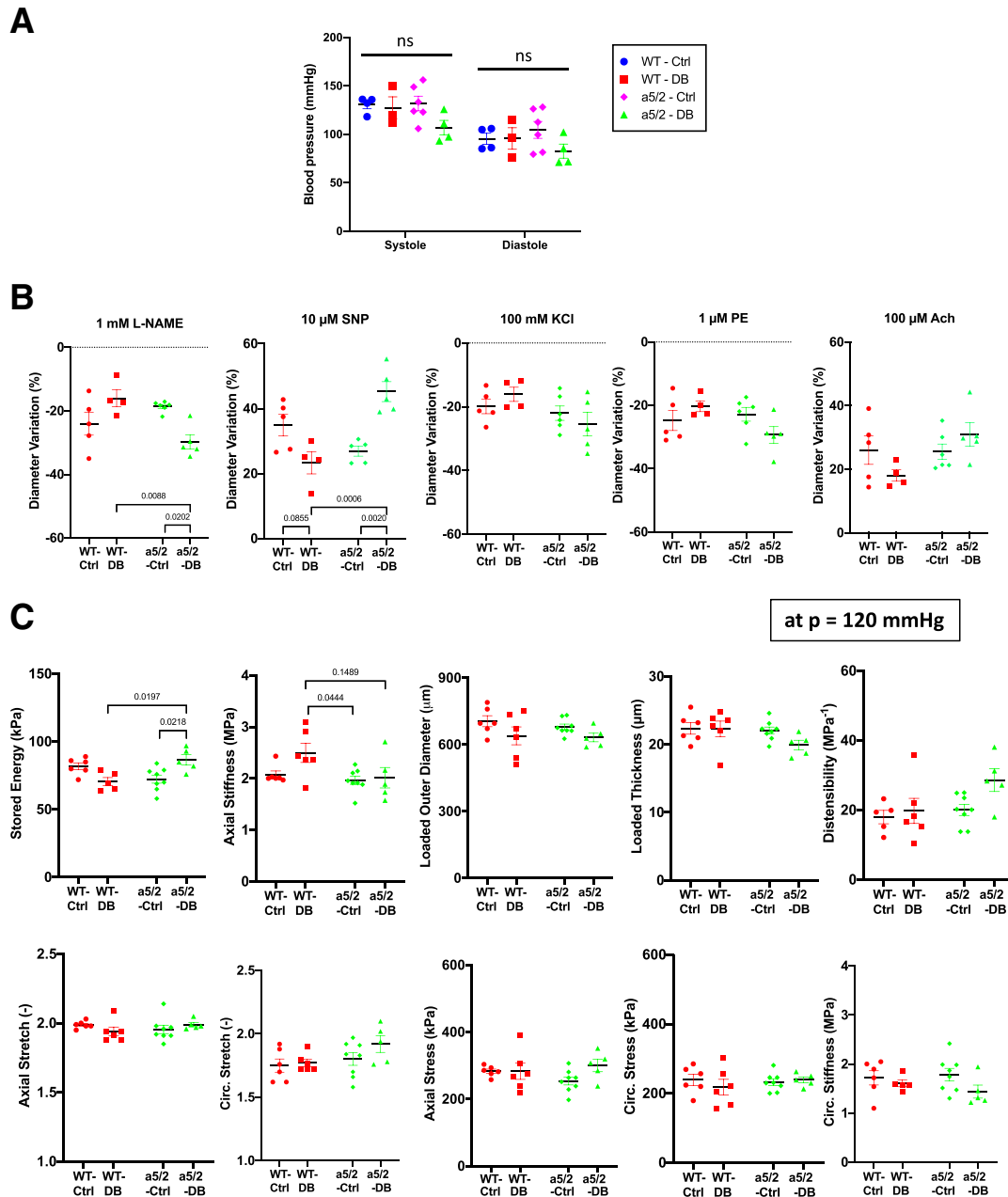


Figure 7—Biomechanical phenotyping of mouse aortas. (A) Systolic and diastolic blood pressure of animals 8 weeks after STZ injection. (B) Change in diameters of carotid arteries during vessel active testing. KCl induces Ca^{2+} dependent membrane depolarization; PE induces EC-independent vessel contraction; acetylcholine (Ach) induces EC-dependent relaxation; L-NAME blocks NO synthase to induce EC-dependent contraction; the NO donor sodium nitroprusside (SNP) induces EC-independent relaxation. (C) Passive mechanics of carotid arteries (calculated at 120 mmHg). WT control, $n = 5$ mice; WT T1D, $n = 4$; integrin $\alpha 5/2$ control, $n = 6$; and T1D integrin $\alpha 5/2$, $n = 5$. Analysis was by two-way ANOVA. Ctrl, control.

WT T1D mice. The calf region showed a similar trend that did not reach statistical significance (Fig. 5A–C). No significant differences were observed among larger arteries (96–240 μm).

To address this discrepancy, we examined muscle from mice that were fixed without vasodilation. Thigh-muscle sections were stained with SMA to identify muscular arteries, including arteries (diameter, 18–150 μm) and arterioles (diameter, 4–18 μm). Calf muscle sections were stained

with CD31 to identify all vessels, including capillaries (diameter, $< 4 \mu\text{m}$). Operated thigh muscle consistently had higher density of muscular arteries than the control thigh (Fig. 6A), consistent with arteriogenesis. The operated thigh of WT T1D mice had fewer arteries compared with WT nondiabetic controls, which was partially rescued by the chimera integrin $\alpha 5/2$ (Fig. 6A and B). Examining capillary density and the ratio of capillary area to total muscle area in the calf by CD31 staining showed an increase in

control mice, which trended lower in WT T1D mice but was rescued by integrin $\alpha 5/2$ T1D (Fig. 6C, D, and E). These results show that the integrin $\alpha 5/2$ mutation attenuated T1D-induced vascular remodeling defects, consistent with the laser Doppler results. Discrepancy of this sort between micro-CT and staining is generally attributed to vasodilation used in micro-CT (36). Inhibition of vascular function, often due to inflammation, will be relieved by vasodilation. These results thus suggest that the $\alpha 5/2$ mutation improves recovery in diabetic conditions mainly by improving vascular function and angiogenesis.

We also considered whether the $\alpha 5/2$ mutation might affect the immediate responses to hypoxia after surgery. We therefore stained calf muscle 24 h after surgery for HIF1 α , VEGFR2, and eNOS phosphorylation, which are induced or activated by hypoxia and critical to recovery from HLI (37,38). Operated tissue had strong increases of phospho-eNOS and phospho-VEGFR2 in the endothelium and HIF1 α in the muscle compared with tissue from unligated control calves (Supplementary Figs. 5–7). However, induction of phospho-eNOS, phospho-VEGFR2, and HIF1 α was indistinguishable between WT T1D– and integrin $\alpha 5/2$ T1D–operated calves (Supplementary Figs. 5–7). Thus, the initial responses to hypoxia were unaffected by integrin $\alpha 5/2$, implying that integrin $\alpha 5/2$ improves later stages of postischemia vascular remodeling in T1D.

Carotid Artery Properties and Mechanical Function

Hyperglycemia, together with the resultant elevated levels of reactive oxygen species, synergistically increase inflammation, advanced glycosylation end products, endothelial cell dysfunction and vessel stiffening (39,40). Because EC dysfunction and large-artery stiffness are both markers or predictors and causative factors in cardiovascular disease (41,42), we characterized biomechanical properties of the carotid arteries. Noting that values of key properties are pressure dependent, we found blood pressures unchanged among WT and integrin $\alpha 5/2$ mice, both control and T1D (Fig. 7A). *Ex vivo* exposure of the excised, pressurized arteries (see *Research Design and Methods*) to 100 mmol/L KCl or phenylephrine induced similar vasoconstriction across all four groups (Fig. 7B). Subsequent exposure to acetylcholine to induce EC-dependent vasorelaxation also revealed modest differences among the four groups, and treatment with the eNOS inhibitor L-NAME resulted in significantly higher vasoconstriction in integrin $\alpha 5/2$ T1D arteries compared with WT T1D arteries, indicating higher NO responses in the chimera integrin background. Responses to the EC-independent NO donor sodium nitroprusside showed a trend toward decreased vasorelaxation in the T1D arteries in WT mice but significantly improved vasorelaxation in the integrin $\alpha 5/2$ T1D arteries relative to WT T1D arteries (Fig. 7B). Together, these results showed that integrin $\alpha 5/2$ improved vascular SMC responses in the T1D setting. Passive mechanical testing showed that increased stiffness in T1D arteries manifested primarily in

the axial direction in most WT mice (the preferred direction of adventitial collagen), but $\alpha 5/2$ tended to normalize this value. Similarly, T1D reduced elastic energy storage (a key mechanical functionality of the artery) in WT mice, which was improved significantly in integrin $\alpha 5/2$ T1D mice (Fig. 7C). These biomechanical results indicate that integrin $\alpha 5/2$ improved multiple aspects of large-artery function in T1D, both active and passive.

DISCUSSION

These data show that in T1D mice, mutation of the cytoplasmic domain of the main FN receptor, integrin $\alpha 5$, substantially reduces atherosclerosis and improves markers of vascular stability. Based on plaque size, the results suggest that FN- $\alpha 5$ signaling accounts for roughly half of the accelerated plaque progression seen in T1D. More strikingly, the integrin $\alpha 5/2$ mutation completely normalized the elevated immune-cell accumulation and MMP expression in the diabetic plaques while leaving smooth muscle and collagen content mostly unchanged. These effects were observed despite the persistently higher levels of plasma cholesterol in diabetic $\alpha 5/2$ mice compared with nondiabetic mice, though triglyceride levels were less elevated in $\alpha 5/2$ mice. The $\alpha 5$ mutation improved both recovery of blood flow after femoral artery ligation and large-artery biomechanical properties, which affect blood flow to many end organs. We conclude that the $\alpha 5/2$ mutation substantially blunts the acceleration of disease in this diabetic model. Decreased levels of triglycerides may contribute to this effect but cell autonomous mechanisms are likely more important. The mechanism of the effect of $\alpha 5/2$ mutation on circulating triglycerides is unclear. It could conceivably involve intestinal transport, uptake in lymphatics, or uptake or secretion in the liver or metabolism in muscle or other tissues. That PDE4D^{mut} mice show no effect argues against cAMP as the mediator. This question thus remains open for future work.

Numerous studies have demonstrated that hyperglycemia increases FN expression in endothelial and SMCs and increases accumulation of FN in vascular basement membranes (4,12–14,16–18). Previous work also found that FN signaling through its integrin receptors promotes vascular inflammation (43,44), limits NO production (45), increases atherosclerotic plaque size (46,47), and impedes flow-dependent vascular remodeling (9,11). FN accumulation in vascular basement membranes was elevated in all the diabetic mice with no differences between WT and integrin $\alpha 5$ or PDE4D^{mut} mice. These results support the complete functionality of the $\alpha 5$ mutant and rules out changes in FN expression or matrix incorporation as causative factors in this setting. Together, these data support the conclusion that increased FN deposition in vascular basement membranes is a major cause of diabetic vascular complications. Interestingly, FN accumulation is reduced in $\alpha 5/2$ compared with WT aortas

after induction of acute hypertension by aortic banding (48), indicating that this effect is stimulus specific.

To our surprise, and in contrast to results for the integrin $\alpha 5/2$ mice, PDE4D^{mut} mice had slightly worse outcomes in T1D. In hyperlipidemia, they exhibited no decrease in plaque size, inflammatory status, or MMP expression relative to WT, diabetic, hyperlipidemic mice. They had reduced smooth muscle content in the plaque, suggestive of vulnerability, though cap thickness and collagen content were not detectably different, which makes this interpretation less compelling. T1D PDE4D^{mut} mice also had reduced blood-flow recovery in the HLI model. Last, they died earlier for reasons that were not determined. The effects of the PDE4D mutation in T1D were thus markedly different from previous findings in nondiabetic mice (10).

The reason for faster recovery from HLI in the $\alpha 5/2$ mice is not entirely clear. Paradoxically, micro-CT, imaged after strong vasodilation, showed fewer vessels in $\alpha 5/2$ mice. However, analysis by immunohistochemistry without vasodilation gave a distinct result. SMA staining showed that the $\alpha 5/2$ mutation partially rescued the decrease in artery density in the thigh of diabetic WT mice. Additionally, PECAM1 staining and capillary density in the calf were greater in $\alpha 5/2$ mice. These data point toward improved vessel remodeling and function, consistent with previous observations in nondiabetic integrin $\alpha 5/2$ mice, where faster recovery from HLI was accompanied by fewer vessels by micro-CT but larger vessels by immunohistochemistry (11). These effects are likely related to the ability of FN to decrease eNOS activation and NO production (45) and to enhance inflammatory signaling (43,44,46). The $\alpha 5/2$ mutation would thus reverse these effects and confer improved vessel function. Indeed, inhibition of NF- κ B in the endothelium yielded a similar pattern, which was attributed to an effect on NO production and vessel function (36). However, further analysis will be required to fully understand the nature of the altered vessel remodeling in these mice in diabetes.

Collectively, these data lead to the conclusion that FN accumulation and signaling through the integrin $\alpha 5$ subunit cytoplasmic domain make a major contribution to accelerated vascular disease in T1D. However, the PDE4D/cAMP pathway that promotes atherosclerosis under normoglycemic conditions appears not to be the key $\alpha 5$ effector in hyperglycemia. Indeed, blocking the $\alpha 5$ -PDE4D interaction had deleterious effects in this T1D model. This result implies that integrin $\alpha 5$ likely has additional effectors that play larger roles in T1D than in normoglycemia. Identification of such pathways and testing the consequences of their inhibition are key directions for future work.

Funding. This work was supported by U.S. Public Health Service (USPHS) grant P01 HL107205 and the Yale Diabetes Research Center (grant P30 DK045735). M.A.S. R.H. was supported by a Chinese Scholar's Fellowship (grant 201606275182). C.F.-H. was supported by USPHS grant R35HL135820.

Duality of Interest. No potential conflicts of interest relevant to this article were reported.

Author Contributions. M.C., and R.H. performed most of the animal work, including mouse handling, dissection, blood collection, tissue preparation and embedding, frozen section cutting and staining, and imaging; performed most data analysis; and wrote the first draft of the manuscript. C.C., and S.-I.M. performed the artery mechanical test and analysis. Z.W.Z. and J.Z. performed femoral artery ligation surgery and micro-CT preparation and imaging. S.Y., K.T., and M.L. contributed to animal work. P.F.T., and A.S. performed TAG and VLDL assays. C.F.-H. provided funding and advice on atherosclerosis experiments and lipid analysis. J.D.H. provided funding and advice on mechanical testing and analysis. M.A.S. conceived and funded the study, revised the manuscript, and accepts official responsibility for the overall integrity of the manuscript (including ethics, data handling, reporting of results, and study conduct).

References

- Schofield J, Ho J, Soran H. Cardiovascular risk in type 1 diabetes mellitus. *Diabetes Ther* 2019;10:773–789
- Petrie JR, Sattar N. Excess cardiovascular risk in type 1 diabetes mellitus. *Circulation* 2019;139:744–747
- Knapp M, Tu X, Wu R. Vascular endothelial dysfunction, a major mediator in diabetic cardiomyopathy. *Acta Pharmacol Sin* 2019;40:1–8
- Ljubimov AV, Burgeson RE, Butkowski RJ, et al. Basement membrane abnormalities in human eyes with diabetic retinopathy. *J Histochem Cytochem* 1996;44:1469–1479
- Moore KJ, Fisher EA. The double-edged sword of fibronectin in atherosclerosis. *EMBO Mol Med* 2012;4:561–563
- Magnusson MK, Mosher DF. Fibronectin: structure, assembly, and cardiovascular implications. *Arterioscler Thromb Vasc Biol* 1998;18:1363–1370
- Rohwedder I, Montanez E, Beckmann K, et al. Plasma fibronectin deficiency impedes atherosclerosis progression and fibrous cap formation. *EMBO Mol Med* 2012;4:564–576
- Dhanesha N, Ahmad A, Prakash P, Doddapattar P, Lentz SR, Chauhan AK. Genetic ablation of extra domain A of fibronectin in hypercholesterolemic mice improves stroke outcome by reducing thrombo-inflammation. *Circulation* 2015;132:2237–2247
- Yun S, Budatha M, Dahlman JE, et al. Interaction between integrin $\alpha 5$ and PDE4D regulates endothelial inflammatory signalling. *Nat Cell Biol* 2016;18:1043–1053
- Yun S, Hu R, Schwaemmle ME, et al. Integrin $\alpha 5\beta 1$ regulates PP2A complex assembly through PDE4D in atherosclerosis. *J Clin Invest* 2019;129:4863–4874
- Budatha M, Zhang J, Zhuang ZW, et al. Inhibiting integrin $\alpha 5$ cytoplasmic domain signaling reduces atherosclerosis and promotes arteriogenesis. *J Am Heart Assoc* 2018;7:e007501
- Labat-Robert J, Kern P, Robert L. Modifications of the biosynthesis of type-I and type-III collagens and fibronectin during diabetes and atherosclerosis. *Z Gerontol* 1991;24:66–69
- Ledet T, Rasmussen LM, Heickendorff L, Barfod K, Thøgersen VB. The nature of large vessel disease in diabetes mellitus. *J Diabet Complications* 1990;4:63–65
- Hill RE, Williams RE. A quantitative analysis of perineurial cell basement membrane collagen IV, laminin and fibronectin in diabetic and non-diabetic human sural nerve. *J Anat* 2002;201:185–192
- To M, Goz A, Camenzind L, et al. Diabetes-induced morphological, biomechanical, and compositional changes in ocular basement membranes. *Exp Eye Res* 2013;116:298–307

Acknowledgments. The authors thank Dr. Kathleen Martin for generously providing PCSK9 virus and thank Dr. Kevan Herold for advice about the diabetes model and critical comments on the manuscript.

16. Cagliero E, Roth T, Roy S, Lorenzi M. Characteristics and mechanisms of high-glucose-induced overexpression of basement membrane components in cultured human endothelial cells. *Diabetes* 1991;40:102–110
17. Chen S, Khan ZA, Cukiernik M, Chakrabarti S. Differential activation of NF- κ B and AP-1 in increased fibronectin synthesis in target organs of diabetic complications. *Am J Physiol Endocrinol Metab* 2003;284:E1089–E1097
18. Cherian S, Roy S, Pinheiro A, Roy S. Tight glycemic control regulates fibronectin expression and basement membrane thickening in retinal and glomerular capillaries of diabetic rats. *Invest Ophthalmol Vis Sci* 2009;50:943–949
19. Roy S, Nasser S, Yee M, Graves DT, Roy S. A long-term siRNA strategy regulates fibronectin overexpression and improves vascular lesions in retinas of diabetic rats. *Mol Vis* 2011;17:3166–3174
20. Roy S, Sato T, Paryani G, Kao R. Downregulation of fibronectin overexpression reduces basement membrane thickening and vascular lesions in retinas of galactose-fed rats. *Diabetes* 2003;52:1229–1234
21. Björklund MM, Hollensen AK, Hagensen MK, et al. Induction of atherosclerosis in mice and hamsters without germline genetic engineering. *Circ Res* 2014;114:1684–1689
22. Gleason RL, Gray SP, Wilson E, Humphrey JD. A multi-axial computer-controlled organ culture and biomechanical device for mouse carotid arteries. *J Biomech Eng* 2004;126:787–795
23. Bellini C, Bersi MR, Caulk AW, et al. Comparison of 10 murine models reveals a distinct biomechanical phenotype in thoracic aortic aneurysms. *J R Soc Interface* 2017;14:20161036
24. Bersi MR, Khosravi R, Wujciak AJ, Harrison DG, Humphrey JD. Differential cell-matrix mechanoadaptations and inflammation drive regional propensities to aortic fibrosis, aneurysm or dissection in hypertension. *J R Soc Interface* 2017;14:20170327
25. Aryal B, Singh AK, Zhang X, et al. Absence of ANGPTL4 in adipose tissue improves glucose tolerance and attenuates atherogenesis. *JCI Insight* 2018;3:97918
26. Daugherty A, Tall AR, Daemen MJAP, et al.; American Heart Association Council on Arteriosclerosis, Thrombosis and Vascular Biology; and Council on Basic Cardiovascular Sciences. Recommendation on design, execution, and reporting of animal atherosclerosis studies: a scientific statement from the American Heart Association. *Arterioscler Thromb Vasc Biol* 2017;37:e131–e157
27. Plutzky J. Atherosclerotic plaque rupture: emerging insights and opportunities. *Am J Cardiol* 1999;84(1A):15J–20J
28. Fuster V, Moreno PR, Fayad ZA, Corti R, Badimon JJ. Atherothrombosis and high-risk plaque: part I: evolving concepts. *J Am Coll Cardiol* 2005;46:937–954
29. Olejarz W, Łacheta D, Kubiak-Tomaszewska G. Matrix metalloproteinases as biomarkers of atherosclerotic plaque instability. *Int J Mol Sci* 2020;21:E3946
30. Heuslein JL, Gorick CM, Price RJ. Epigenetic regulators of the revascularization response to chronic arterial occlusion. *Cardiovasc Res* 2019;115:701–712
31. Schiekofer S, Galasso G, Sato K, Kraus BJ, Walsh K. Impaired revascularization in a mouse model of type 2 diabetes is associated with dysregulation of a complex angiogenic-regulatory network. *Arterioscler Thromb Vasc Biol* 2005;25:1603–1609
32. Hazarika S, Dokun AO, Li Y, Popel AS, Kontos CD, Annex BH. Impaired angiogenesis after hindlimb ischemia in type 2 diabetes mellitus: differential regulation of vascular endothelial growth factor receptor 1 and soluble vascular endothelial growth factor receptor 1. *Circ Res* 2007;101:948–956
33. Landázuri N, Joseph G, Guldberg RE, Taylor WR. Growth and regression of vasculature in healthy and diabetic mice after hindlimb ischemia. *Am J Physiol Regul Integr Comp Physiol* 2012;303:R48–R56
34. Tamarat R, Silvestre JS, Huijberts M, et al. Blockade of advanced glycation end-product formation restores ischemia-induced angiogenesis in diabetic mice. *Proc Natl Acad Sci USA* 2003;100:8555–8560
35. Yu J, Dardik A. A murine model of hind limb ischemia to study angiogenesis and arteriogenesis. *Methods Mol Biol* 2018;1717:135–143
36. Tirziu D, Jaba IM, Yu P, et al. Endothelial nuclear factor- κ B-dependent regulation of arteriogenesis and branching. *Circulation* 2012;126:2589–2600
37. Patel TH, Kimura H, Weiss CR, Semenza GL, Hofmann LV. Constitutively active HIF-1 α improves perfusion and arterial remodeling in an endovascular model of limb ischemia. *Cardiovasc Res* 2005;68:144–154
38. Amano K, Matsubara H, Iba O, et al. Enhancement of ischemia-induced angiogenesis by eNOS overexpression [retracted in: *Hypertension* 2013;62:e3]. *Hypertension* 2003;41:156–162
39. Lu S, Liao Z, Lu X, et al. Hyperglycemia acutely increases cytosolic reactive oxygen species via O-linked GlcNAcylation and CaMKII activation in mouse ventricular myocytes. *Circ Res* 2020;126:e80–e96
40. Rubin J, Nambi V, Chambless LE, et al. Hyperglycemia and arterial stiffness: the Atherosclerosis Risk in the Communities study. *Atherosclerosis* 2012;225:246–251
41. Hadi HA, Carr CS, Al Suwaidi J. Endothelial dysfunction: cardiovascular risk factors, therapy, and outcome. *Vasc Health Risk Manag* 2005;1:183–198
42. Kozakova M, Palombo C. Diabetes mellitus, arterial wall, and cardiovascular risk assessment. *Int J Environ Res Public Health* 2016;13:201
43. Orr AW, Sanders JM, Bevard M, Coleman E, Sarembock IJ, Schwartz MA. The subendothelial extracellular matrix modulates NF- κ B activation by flow: a potential role in atherosclerosis. *J Cell Biol* 2005;169:191–202
44. Hahn C, Orr AW, Sanders JM, Jhaveri KA, Schwartz MA. The subendothelial extracellular matrix modulates JNK activation by flow. *Circ Res* 2009;104:995–1003
45. Yurdagul A Jr, Chen J, Funk SD, Albert P, Kevil CG, Orr AW. Altered nitric oxide production mediates matrix-specific PAK2 and NF- κ B activation by flow. *Mol Biol Cell* 2013;24:398–408
46. Yurdagul A Jr, Green J, Albert P, McInnis MC, Mazar AP, Orr AW. α 5 β 1 integrin signaling mediates oxidized low-density lipoprotein-induced inflammation and early atherosclerosis. *Arterioscler Thromb Vasc Biol* 2014;34:1362–1373
47. Al-Yafeai Z, Yurdagul A Jr, Peretik JM, Alfaidi M, Murphy PA, Orr AW. Endothelial FN (fibronectin) deposition by α 5 β 1 integrins drives atherogenic inflammation. *Arterioscler Thromb Vasc Biol* 2018;38:2601–2614
48. Budatha M, Zhang J, Schwartz MA. Fibronectin-mediated inflammatory signaling through integrin α 5 in vascular remodeling. *J Am Heart Assoc* 2021;10:e021160